J. Fluid Mech. (1991), *vol.* 233, *pp.* 661–689
Printed in Great Britain

Final equilibrium state of a two-dimensional shear layer

By J. SOMMERIA[1], C. STAQUET[1] AND R. ROBERT[2]

[1] Laboratoire de Physique, Ecole Normale Supérieure de Lyon, 46 al.d'Italie, 69 364 Lyon, France

[2] 21, Avenue Plaine Fleurie 38240 Meylan, France

(Received 6 December 1990 and in revised form 17 June 1991)

We test a new statistical theory of organized structures in two-dimensional turbulence by direct numerical stimulations of the Navier–Stokes equations, using a pseudo-spectral method. We apply the theory to the final equilibrium state of a shear layer evolving from a band of uniform vorticity: a relationship between vorticity and stream function is predicted by maximizing an entropy with the constraints due the constants of the motion. A partial differential equation for the stream function is then obtained. In the particular case of a very thin initial vorticity band, the Stuart's vortices appear to be a family of solutions for this equation. In more general cases we do not solve the equation, but we test the theory by inspecting the relationship between stream function and vorticity in the final equilibrium state of the numerical computation. An excellent agreement is obtained in regions with strong vorticity mixing. However, local equilibrium is obtained before a complete mixing can occur in the whole fluid domain.

1. Introduction

A statistical theory for the emergence of organized structures in two-dimensional turbulence has been proposed by Robert (1989, 1990, 1991) and discussed in Robert & Sommeria (1991). The aim of the present paper is to apply this theory to a simple case and test it by direct numerical simulations. The theory involves the Euler equation and, in its simplest form, applies to an initial condition with piecewise uniform vorticity. The boundaries of the patches become in general more and more intricate as time goes on, but the area of each vorticity patch is conserved, as well as the total kinetic energy of the system. The goal of the theory is to predict the final state, at the end of the cascade processes.

Since the vorticity contours become so intricate, we are not really interested in the exact vorticity field. Indeed the velocity field results from an integration of the vorticity, so that it does not depend on the fine-scale fluctuations of the vorticity: it depends only on its local average. In fact, to exploit all the information given by the constants of the motion, we are led to consider a macroscopic description of the system by introducing the local probability distribution of the different vorticity levels in a small neighbourhood. Therefore we define a macroscopic state as a field of these local probabilities, while an exact vorticity field is called here a microscopic state. We consider all the vorticity fields with the same constants of the motion as the initial condition. It was proved by Robert (1989) that 'most' of these possible microscopic states are very 'close' to a well-defined macroscopic state. This state is obtained by maximizing an entropy functional, with the constraints due to all the

constants of the motion. The theory predicts a well-defined relationship between the locally averaged vorticity and the stream function. Therefore this averaged vorticity field is a steady solution of the Euler equation. In the presence of a very small viscosity, the local vorticity fluctuations are smoothed out, and this locally averaged vorticity becomes the actual steady flow which emerges from turbulence.

A direct numerical test of the theory, using Euler equations, would be limited by the production of vorticity structures at increasing fine scales, which become rapidly out of reach of any numerical scheme. Therefore, with any numerical method, a subgrid-scale modelling is needed to compute the long-time behaviour. Such modelling should be able to smear out correctly the local vorticity fluctuations, while conserving the total energy and circulation. In the absence of any known subgrid-scale modelling with these properties, we choose an ordinary viscosity, therefore solving the Navier–Stokes equations. The Laplacian term locally averages vorticity, and the total energy decays only moderately when viscosity is small. We test the theory in the case of a shear layer, in which the initial vorticity is uniform and limited to a band (with smoothed edges). The development of the shear instability and merging processes strongly mix the vorticity with the surrounding irrotational fluid. (This has been described in great detail by Corcos & Sherman 1984). Then a final vortex is formed, which is nearly a steady solution of the Euler equation (very slowly diffusing by viscosity). Since the boundary conditions are periodic in the direction of the initial band, this final vortex is in fact a periodic chain of vortices. This geometry is chosen for its simplicity, but it is similar to an annular geometry. Such annular shears are found in laboratory experiments (for instance Sommeria, Meyers & Swinney 1988; Antipov *et al.* 1986; Rabaud & Couder 1983) and in the atmosphere of giant planets like Jupiter.

The theory is applied to a shear layer in §2, and the relationship between vorticity and stream function is predicted for the final vortex. This partial differential equation can be solved explicitly in the particular case of a wide domain, and yields the family of vortex chains found by Stuart (1967). We compare the theoretical relationship with the numerical results in §3.

2. Statistical equilibrium states

2.1. *Equations and constants of the motion*

We study the particular case of a 2π-periodic fluid motion in the x-variable confined to a strip $-L \leqslant y \leqslant +L$. We denote the fluid domain $\Omega =]0, 2\pi[\times]-L, +L[$. Then the velocity $\boldsymbol{u}(t, x, y) = (u, v)$ and normal vorticity component ω are 2π-periodic in the x-variable and satisfy

$$\omega_t + \nabla \cdot (\omega \boldsymbol{u}) = 0, \quad \omega(0, \boldsymbol{x}) = \omega_0(\boldsymbol{x}), \tag{1}$$

$$\nabla \times \boldsymbol{u} = \omega, \tag{2}$$

$$\nabla \cdot \boldsymbol{u} = 0, \quad v = 0 \text{ at the boundaries } y = \pm L$$

One can check that the functionals

$$E_c = \frac{1}{2}\int_\Omega \boldsymbol{u}^2 \,\mathrm{d}\boldsymbol{x}, \quad I_f = \int_\Omega f(\omega(\boldsymbol{x}))\,\mathrm{d}\boldsymbol{x}, \quad P = \int_\Omega u \,\mathrm{d}\boldsymbol{x}, \quad M = \int_\Omega y\omega(\boldsymbol{x})\,\mathrm{d}\boldsymbol{x}$$

are constants of the motion. The functionals I_f are constructed from any continuous function f of the vorticity; taking $f(\omega) = \omega^n$, we get the conservation of the moment

$$\Gamma_n = \int_\Omega \omega^n \,\mathrm{d}\boldsymbol{x}.$$

Γ_1 is the total circulation around the fluid domain, while $\frac{1}{2}\Gamma_2$ is called the enstrophy. The kinetic energy E_c and the integrals I_f are conserved in the general case of any domain Ω. By contrast the conservation of the physical momentum P and the vorticity momentum M are specific for our channel geometry. The conservation of P results from the absence of global pressure forces in the x-direction, due to the periodic boundary conditions (and can be derived from the Euler equations written in terms of velocity and pressure). The momentum M differs from the physical momentum P by a boundary term (which appears in an integration by parts):

$$M = P - L\int_0^{2\pi} (u(x, -L) + u(x, +L))\,\mathrm{d}x. \tag{3}$$

The conservation of M can be derived directly from (1) and (2) as follows:

$$\frac{\mathrm{d}}{\mathrm{d}t}\int_\Omega y\omega\,\mathrm{d}\boldsymbol{x} = \int_\Omega y\omega_t\,\mathrm{d}\boldsymbol{x} = -\int_\Omega y\nabla\cdot(\omega\boldsymbol{u})\,\mathrm{d}\boldsymbol{x} = -\int_\Omega y\partial_x(\omega u)\,\mathrm{d}\boldsymbol{x} - \int_\Omega y\partial_y(\omega v)\,\mathrm{d}\boldsymbol{x}.$$

The first term is equal to zero because of the periodic boundary conditions, and the second term can be rearranged after integration by parts, taking into account that $v = 0$ at $y = \pm L$; then

$$\frac{\mathrm{d}M}{\mathrm{d}t} = \int_\Omega \omega v\,\mathrm{d}\boldsymbol{x}$$

but $\omega = \partial_x v - \partial_y u$ from which

$$\frac{\mathrm{d}M}{\mathrm{d}t} = \int_\Omega \partial_x(\tfrac{1}{2}v^2)\,\mathrm{d}\boldsymbol{x} - \int_\Omega v\,\partial_y u\,\mathrm{d}\boldsymbol{x}.$$

The periodicity condition implies that the first term is equal to zero, and after integration by parts the second term gives

$$\frac{\mathrm{d}M}{\mathrm{d}t} = \int_\Omega u\,\partial_y v\,\mathrm{d}\boldsymbol{x} = -\int_\Omega u\,\partial_x u\,\mathrm{d}\boldsymbol{x} = -\int_\Omega \partial_x(\tfrac{1}{2}u^2)\,\mathrm{d}\boldsymbol{x} = 0,$$

where we have used the relation of incompressibility.

To apply the theory, we need to describe the motion in terms of vorticity. However, $\boldsymbol{u}$ is only defined up to an additive constant on the component u by (2). But $\boldsymbol{u}$ is uniquely determined from the vorticity field if we fix the value of the momentum P. When the initial vorticity field ω_0 and momentum P are given, then the vorticity equations (1) and (2) determine the dynamics of the system.

We now introduce the stream function ψ by

$$u = \partial\psi/\partial y, \qquad \psi = P/4\pi \quad \text{on} \quad y = +L, \quad \psi = -P/4\pi \quad \text{on} \quad y = -L;$$
$$v = -\partial\psi/\partial x, \qquad \psi \quad \text{is} \quad 2\pi x\text{-periodic.}$$

A straightforward computation gives

$$E_c = \tfrac{1}{2}\int_\Omega \boldsymbol{u}^2\,\mathrm{d}\boldsymbol{x} = \tfrac{1}{2}\int_\Omega \psi\omega\,\mathrm{d}\boldsymbol{x} + \frac{P}{8\pi}(P - M);$$

therefore the conservation of the kinetic energy is equivalent to the conservation of the functional

$$E = \tfrac{1}{2}\int_\Omega \psi\omega\,\mathrm{d}\boldsymbol{x}.$$

2.2. *The state of maximum entropy*

We consider an initial condition with one or several vortex patches with a single uniform vorticity level $\omega = a$ surrounded by irrotational fluid. In the absence of viscosity the flow will contain the two levels of vorticity a and 0 forever, but in general the boundaries of the patches will become more and more intricate. Therefore a complete description of the system will require increasingly more information, so that such a microscopic description will become more and more difficult and useless. We define then the probability $e(\boldsymbol{x})$ of finding the vorticity level a in a small neighbourhood of a location $\boldsymbol{x}$. The probability of finding the vorticity 0 will be the complementary $1-e(\boldsymbol{x})$. The probability field $e(\boldsymbol{x})$ represents our macrostate. In the presence of a very small viscosity, we can expect that the inertial filamentation process is preserved, but the resulting fine-scale vorticity structures are then smoothed out, leading to the locally averaged vorticity field $\bar{\omega}(\boldsymbol{x}) = ae(\boldsymbol{x})$. In our particular case of an initial condition with a single non-zero vorticity level a, the local probability distribution is completely determined by its average, but this would not be true in more general cases.

As discussed in Robert & Sommeria (1991), the system is most likely to reach a neighbourhood of the macroscopic state which maximizes the entropy

$$S = -\int_\Omega [e\log e + (1-e)\log(1-e)]\,\mathrm{d}\boldsymbol{x} \tag{4}$$

with the constraints due to the constants of the motion. We write these constraints in terms of the locally averaged vorticity $\bar{\omega}(\boldsymbol{x}) = ae(\boldsymbol{x})$ and the associated stream function Ψ, defined by $-\nabla^2\Psi = \bar{\omega}$ (with the above boundary conditions).

$$\int_\Omega \bar{\omega}\,\mathrm{d}\boldsymbol{x} = \Gamma_1, \quad \frac{1}{2}\int_\Omega \Psi\bar{\omega}\,\mathrm{d}\boldsymbol{x} = E, \quad \int_\Omega y\bar{\omega}\,\mathrm{d}\boldsymbol{x} = M.$$

We do not have to take into account the fourth constant of the motion P, as it is now fixed in order to define the dynamical system. In this particular case of a single non-zero vorticity level a, the conservation of the functionals $I_f(\omega)$ reduces to the conservation of the total area of the patches with level $\omega = a$, which is also the circulation Γ_1 around the domain Ω, divided by a.

The variational problem is solved by introducing the Lagrange multipliers α, β, γ corresponding to the three independent constraints, so that the first variations satisfy, for any small variation $\delta e(\boldsymbol{x})$ of the probability field $e(\boldsymbol{x})$:

$$\delta S - \alpha\,\delta\Gamma_1 - \beta\delta E - \gamma\delta M = 0.$$

These variations must be expressed in terms of the variation $\delta e(\boldsymbol{x})$. To express the boundary term, δE can be rearranged by part integration, using (3):

$$\delta E = \frac{1}{2}\left(\int_\Omega \delta\Psi\bar{\omega}\,\mathrm{d}\boldsymbol{x} + \int_\Omega \delta\bar{\omega}\Psi\,\mathrm{d}\boldsymbol{x}\right) = \int_\Omega \delta\bar{\omega}\Psi\,\mathrm{d}\boldsymbol{x} + \frac{P}{8\pi}\frac{\delta(P-M)}{L}.$$

Since $\delta P = 0$, the boundary term reduces to $-(P/8\pi)(\delta M/L)$. The variations δS, $\delta\Gamma_1$ and δM are obtained by straightforward differentiation, which leads to

$$\int_\Omega \left[\log\left(\frac{e}{1-e}\right) + \alpha a + \beta a\Psi + \left(\gamma - \frac{\beta P}{8\pi L}\right)ay\right]\delta e(\boldsymbol{x})\,\mathrm{d}\boldsymbol{x} = 0$$

for any small variation $\delta e(\boldsymbol{x})$. Now $e(\boldsymbol{x})$ and $\Psi(\boldsymbol{x})$ denote the optimal fields. For this

relation to be satisfied for any variation $\delta e(x)$, the integrand must vanish, which leads to

$$e(x,y) = \frac{\exp\{-\alpha a - \beta a[\Psi + (\gamma'/\beta)y]\}}{1+\exp\{-\alpha a - \beta a[\Psi + (\gamma'/\beta)y]\}}, \quad \text{with} \quad \gamma' = \gamma - \frac{\beta P}{8\pi L}. \tag{5}$$

Using the relation $-\nabla^2\Psi = ae$, we obtain a differential equation for the macroscopic stream function Ψ:

$$-\nabla^2\Psi = \frac{a\exp\{-\alpha a - \beta a[\Psi + (\gamma'/\beta)y]\}}{1+\exp\{-\alpha a - \beta a[\Psi + (\gamma'/\beta)y]\}}, \quad \Psi = \pm\frac{P}{4\pi} \quad \text{on} \quad y = \pm L. \tag{6}$$

It is convenient to make the change of stream function $\phi = \Psi + (\gamma'/\beta)y$ which corresponds to a change of reference frame, the new frame translating with uniform speed along the x-axis. In this frame of reference, the vorticity is a function of the stream function, so that the locally averaged vorticity field appears to be a steady solution of the Euler equations. In the presence of a very small viscosity, we expect that the fine-scale fluctuations will be smeared out, so that this steady flow becomes the actual final state of the system.

Denoting $\theta = \exp(\alpha a)\,\phi/a$, we get

$$-\nabla^2\theta = \frac{\exp(\lambda\theta)}{1+\mu\exp(\lambda\theta)}, \quad \theta = \pm B \quad \text{on} \quad y = \pm L, \tag{7}$$

where

$$\lambda = -a^2\beta\exp(-\alpha a), \quad \mu = \exp(-\alpha a), \quad B = \left(\frac{P}{4\pi} + \frac{\gamma'}{\beta}L\right)\frac{\exp(\alpha a)}{a}.$$

Notice that the second term of (7) can also be written as an hyperbolic tangent of a linear function of θ. Particularly interesting is the case $B = 0$ which corresponds to a zero mean velocity in the moving frame. This case has been mathematically studied by T. Dumont & Shatzman (1991, paper in preparation). It has been shown that there is some value μ^* such that for $\mu < \mu^*$, there is a critical value $\lambda_c(\mu)$ of the parameter λ satisfying:

for $\lambda < \lambda_c$, the problem has a unique solution which depends only on the y variable;

for $\lambda = \lambda_c$, a bifurcation occurs with breaking of the x invariance and the appearance of two branches of solutions. This case corresponds to the formation of an organized structure.

The conditions (6) or (7) ensures the vanishing of the first-order variation, which defines a critical point; it is only a necessary condition for a distribution $e(x)$ to be a maximum of entropy. To prove that the critical point is a local maximum of entropy, it is sufficient to check in addition that the second-order variation of the functional (the 'free energy')

$$J[e] = S[e] - \alpha\Gamma_1[e] - \beta E[e] - \gamma M[e]$$

is negative for any small variation $\delta e(x)$ which does not change the constraints at first order. A Taylor expansion yields the second-order variation ($\delta^2 M$ and $\delta^2\Gamma_1$ vanish)

$$\delta^2 J = -\frac{1}{2}\int_\Omega \frac{(\delta e)^2}{e(1-e)}\,\mathrm{d}x - \tfrac{1}{2}\beta\int_\Omega \delta\Psi\,\delta\bar{\omega}\,\mathrm{d}x. \tag{8}$$

The integral of the second term can be written as $\int_\Omega (\nabla\delta\Psi)^2\,\mathrm{d}x$, which is positive. Therefore when β is positive, $\delta^2 J$ is always negative, so that the critical point gives a local maximum of the entropy. For $\beta < 0$, $\delta^2 J$ can be majored by introducing the

first eigenvalue of the Laplacian in the domain Ω, $\kappa_1 = \pi^2/4L^2$ (with boundary condition 0 at $y = \pm L$ and 2π x-periodicity). We then use the well-known inequality

$$\int_\Omega \delta\Psi\,\delta\bar{\omega}\,(\mathrm{d}\boldsymbol{x} \leqslant \frac{1}{\kappa_1}\int_\Omega (\delta\bar{\omega})^2\,\mathrm{d}\boldsymbol{x},$$

which implies, taking into account that e and $1-e$ are smaller than 1,

$$\delta^2 J \leqslant -\frac{1}{2}\left(1+\frac{\beta a^2}{\kappa_1}\right)\int_\Omega (\delta e)^2\,\mathrm{d}\boldsymbol{x}.$$

Therefore the free energy still has a unique maximum when $\beta > -\kappa_1/a^2$. This condition will be refined in the particular case studied in the next sub-section.

2.3. *Explicit solutions in the case of dilute vorticity*

We consider here the particular case of dilute vorticity, defined by the condition $e(\boldsymbol{x}) \ll 1$ everywhere. We expect this to occur when the initial vorticity patch has a small area, for instance a very thin vorticity strip, and becomes strongly diluted among the surrounding irrotational fluid. In this case, the denominator in (5) is close to 1, and the resulting non-dimensional equation (7) simplifies to

$$-\nabla^2\theta = \exp(\lambda\theta). \tag{9}$$

The same equation is also obtained from Onsager's statistical theory of point vortices (Onsager 1949), when the vortex density is locally averaged, using the method of Montgomery & Joyce (1974).

Equation (9) was studied in the nineteenth century (see references in Stuart 1967) and families of explicit solutions have been found by Liouville (1853). We first consider the case with no mean translation along the x-axis ($B = 0$), that is $\theta = 0$ at $y = \pm L$.

For $\lambda < 0$ (i.e. $\beta > 0$) the solution of (9) was shown to be unique (see §2.2); it is thus x-independent, owing to the translational symmetry in x, and it has vorticity extrema at the boundaries $y = \pm L$. Therefore solutions with $\lambda < 0$ are strongly controlled by the boundaries and are not appropriate for a free shear layer. We then restrict the analysis to $\lambda > 0$. We easily check that the solutions of (9) which do not break the translational symmetry are then

$$\exp(\lambda\theta) = 2q^2/[\lambda\cosh^2(qy)], \tag{10}$$

where q is a positive parameter related to λ by

$$\lambda = 2q^2/[\cosh^2(qL)]. \tag{11}$$

This function of q is increasing for small q and decreasing for large q, with a maximum such that $qL\tanh(qL) = 1$ ($qL \approx 1.1997$). Therefore there is no solution of (9) with translational symmetry beyond a critical value of λ, $\lambda_\mathrm{m} \approx 0.8785/L^2$. For $\lambda < \lambda_\mathrm{m}$, there are two solutions corresponding to the two roots of (11). The solution with small q has a widely spread vorticity, while the solution with large q corresponds to a narrow shear layer at $y = 0$.

A less straightforward family of solutions of (9) has been studied by Stuart (1967) in the context of shear-layer instability (it is a particular case of Liouville's solutions) and is written in our notation

$$\exp(\lambda\theta) = \frac{2k^2}{\lambda(C\cosh(ky)+A\cos(kx))^2}, \quad \begin{cases} C^2-A^2 = 1, \\ C \geqslant 1, \quad k \text{ integer} \end{cases} \tag{12}$$

These solutions represent an x-periodic array of vortices. When the parameter A is varied this flow deforms continuously from a unidirectional shear ($A = 0$) to an array

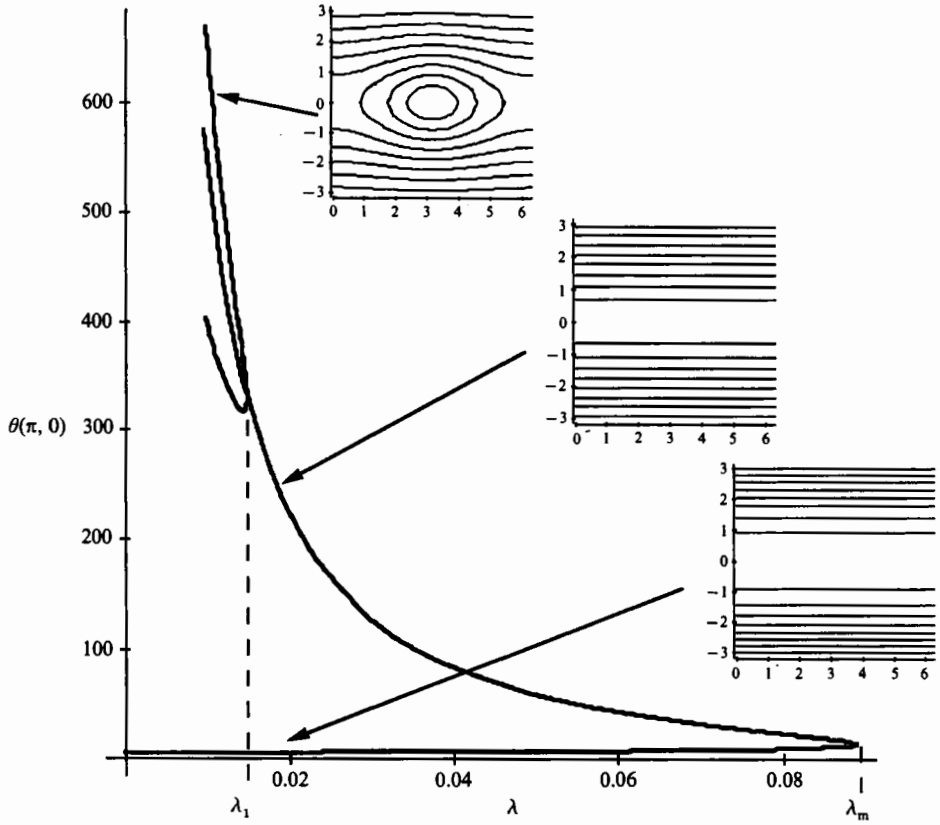

FIGURE 1. Bifurcation diagram for the solutions of (7) in the dilute case $\mu = 0$. The stream function θ at $(x, y) = (\pi, 0)$ is plotted versus λ for the main branch (10) and the first bifurcated branch (12) with $k = 1$. The streamlines at the points indicated by the arrows are shown. The higher-order bifurcations ($k \geqslant 2$) are very close to the $\lambda = 0$ axis and are not represented. The bifurcated solutions correspond to the approximation of large width L.

of point vortices (A infinite). These solutions correspond in fact to an infinite domain in the y-direction, but the impermeability boundary conditions at $y = \pm L$ are nearly satisfied when the width L is sufficiently large. Indeed the slope of the streamlines at $y = \pm L$ is

$$\left|\frac{v}{u}\right| = \frac{A|\sin(kx)|}{C\sinh(kL)} \leqslant \frac{1}{\sinh(kL)},$$

which becomes very small for large L. Then for large $|y|$

$$\lambda\theta \approx \log\left(\frac{2k^2}{\lambda C^2}\right) - 2\log\cosh(ky)$$

so that θ vanishes at the boundaries $y = \pm L$ if

$$C = (2/\lambda)^{\frac{1}{2}}k/\cosh(kL). \tag{13}$$

We deduce from the condition $C \geqslant 1$ that the family of solutions (10) exists only for $\lambda \leqslant \lambda_k = 2k^2/\cosh^2(kL)$. Equality corresponds to (11) with $q = k$, so that family (12) joins the family (10) at the bifurcation point λ_k corresponding to $q = k$. These different solutions can be represented in a bifurcation diagram (figure 1) with the stream function θ at $(x, y) = (\pi, 0)$ versus λ. The main branch, corresponding to

family (10), starts at $\lambda = 0$, goes through the turning point at $\lambda = \lambda_m$, and goes back toward the axis $\lambda = 0$. The parameter q is monotonically increasing along this path. We have only represented the first bifurcated branch, corresponding to family (12) with $k = 1$. The higher successive bifurcated branches ($k \geqslant 2$) would be much closer to the axis $\lambda = 0$. Actually (12) gives only the upper part of the bifurcated branch, while the lower part corresponds to the same kind of solution, translated by a distance π along the x-axis. In fact, the family of bifurcated solutions should be represented by an 'umbrella' corresponding to all the possible phases in x, instead of only two lines.

Solutions with $B \neq 0$ can be obtained by shifting the origin of y, replacing y by $y - y_0$ in (10) and (12). Therefore the influence of this parameter B is trivial, and we shall assume that $B = 0$ for simplicity. It can be shown as a general theorem (Gidas, Ni & Nirenberg 1979) that the solution cannot break the $y \to -y$ symmetry (this is true for any positive second member in an equation of the type (7) or (9)). It can only break the translational symmetry along the x-direction.

We need now to determine the states of maximum entropy among the different solutions of (9) with $\lambda > 0$. This is a difficult task that we have performed only partially. We restrict the discussion to the main branch in the symmetric case $B = 0$. We first introduce solution (10) in (8) for the second variation and use (7) for the non-dimensional variables:

$$\delta^2 J = -\tfrac{1}{2}\lambda \exp(-\alpha a)^{\frac{1}{2}} \int_\Omega [(-\nabla^2 \delta\theta)^2 \frac{\cosh^2(qy)}{2q^2} - (\delta\theta)(-\nabla^2 \delta\theta)]\, \mathrm{d}\boldsymbol{x},$$

where

$$\delta\theta = \frac{\exp(\alpha a)}{a} \delta\Psi.$$

Now the majoration of the previous section becomes

$$\delta^2 J \leqslant -\tfrac{1}{2}\lambda \exp(-\alpha a)^{\frac{1}{2}} \int_\Omega \left(\frac{\cosh^2(qy)}{2q^2} - \frac{1}{\tau_1}\right)(-\nabla^2 \delta\theta)^2\, \mathrm{d}\boldsymbol{x}.$$

Since $\cosh^2(qy) \geqslant 1$ this expression is negative when $q^2 L^2 < \frac{1}{8}\pi^2$. Therefore the main branch corresponds to a maximum of entropy at least for $qL < \pi/\sqrt{8}$.

Choosing a particular perturbation, we show now that the main branch is not an entropy maximum beyond $q = 1$. Let us chose a perturbation $\delta\theta = \cos x/\cosh y$. This perturbation does not modify the total circulation and the energy at first order, as required. The expression for the second variation then becomes

$$\delta^2 J = -2\pi\lambda \exp^{(-\alpha a)} \int_0^L \left(\frac{\cosh^2(qy)}{q^2 \cosh^2 y} - 1\right) \frac{1}{\cosh^4 y}\, \mathrm{d}y.$$

A numerical computation shows that, in the limit of large width L, $\delta^2 J$ is positive between $q = 1$ and $q \approx 2.1$, so that the critical point is not a local maximum of the entropy. In this sense, the velocity profiles with q between 1 and 2.1 are unstable with respect to the perturbation with wavenumber 1. For $q > 2$, we can do the same calculation with a perturbation in $\cos(nx)$ (where n is an integer greater than 1), and find a 'band of instability' for q between n and $2.1n$. Therefore the zonal flow is unstable for any q strictly greater than 1, and a range of 'unstable' wavenumbers is found between $n = q$ and $n = q/2.1$.

We can conjecture that the main branch is an entropy maximum below the bifurcation, for any $q < 1$, but we were not able to prove it. Notice that a linear

stability analysis of the velocity profile (10) using Rayleigh's equation yields a threshold of instability at $q = 1$. Indeed, all the unstable modes have a wavenumber smaller than q (see for instance Drazin & Reid 1981), and if $q < 1$, those unstable modes are prohibited by the periodic boundary conditions. Therefore a change of stability at $q = 1$, according to the point of view of entropy maximum, would be quite in agreement with the linear stability analysis.

By continuity the second bifurcated branch ($k = 2$) must inherit the property of instability of the main branch near $q = 2$. Since an instability already occurs at a wavenumber 1, we have then an interpretation of the pairing mechanism in terms of entropy. Notice however that this second bifurcated branch could become stable far from the main branch.

The Lagrange parameters α and β have to be determined from the initial conditions by writing the equality of the constants of the motion in the final equilibrium state and in the initial state. Therefore we need to calculate the circulation Γ_1 and kinetic energy E_c corresponding to (10) and (12). For simplicity we limit ourselves to the symmetric case $B = 0$, for which the momentum M vanishes:

$$\Gamma_1 = a\exp(-\alpha a)\int_\Omega -\nabla^2\theta\,\mathrm{d}\boldsymbol{x} = a\exp(-\alpha a)\int_0^{2\pi}[(-\partial_y\theta)_{y=L}+(\partial_y\theta)_{y=-L}]\,\mathrm{d}\boldsymbol{x},$$

$$E_c = a\exp(-\alpha a))^2\left(\frac{1}{2}\int_\Omega(\partial_y\theta)^2\,\mathrm{d}\boldsymbol{x}+\frac{1}{2}\int_\Omega(\partial_x\theta)^2\,\mathrm{d}\boldsymbol{x}\right).$$

We now calculate Γ_1 and E_c for the family (12). For large values of kL, the circulation is

$$\Gamma_1 = a\exp_{(-\alpha a)}8\pi k/\lambda.$$

To calculate the energy, we integrate the contribution of each velocity component first along the x-direction, then along the y-direction (with $Y = ky$), taking the limit of large kL:

$$\frac{1}{2}\int_\Omega(\partial_x\theta)^2\,\mathrm{d}\boldsymbol{x} = \frac{4k\pi}{\lambda^2}\int_{-kL}^{+kL}\left(\frac{C\cosh Y}{(C^2\sinh^2 Y+1)^{\frac{1}{2}}}-1\right)\mathrm{d}Y \approx \frac{8\pi k}{\lambda^2}\log C,$$

$$\frac{1}{2}\int_\Omega(\partial_y\theta)^2\,d\boldsymbol{x} = \frac{4k\pi}{\lambda^2}C^3\int_{-kL}^{+kL}\frac{\sinh^2 Y\cosh Y}{(C^2\sinh^2 Y+1)^{\frac{3}{2}}}\mathrm{d}Y \approx \frac{8\pi k}{\lambda^2}(\log C+kL-1).$$

In the symmetric case $M = 0$, the final state depends in general on three parameters determined by the initial condition: the initial vorticity level a, the circulation Γ_1, and the kinetic energy E_c. The dilute case corresponds to the limit of very large a, keeping a finite circulation (so that the area of the initial vorticity patches tends to zero). Then the circulation Γ_1 can be considered as a scaling parameter that sets the typical velocity, while the non-dimensional ratio

$$\mathscr{E} = \frac{E_c}{\Gamma_1^2} = \frac{1}{8\pi}\left(L-\frac{1}{k}+\frac{2\log C}{k}\right) \tag{14}$$

characterizes the flow structure. For the x-independent solution, this ratio becomes

$$\mathscr{E} = \frac{1}{8\pi}\left(L-\frac{1}{q}\right). \tag{15}$$

We notice that since $k \geqslant 1$ and $C \geqslant 1$, $\mathscr{E}$ given by (14) is always greater than $(L-1)/8\pi$. Therefore, if $\mathscr{E}$ is smaller than this threshold, we predict an x-independent

final equilibrium state, with q given by (15) (which yields $q < 1$). For $\mathscr{E} > (L-1)/8\pi$ we could have either an x-independent solution with $q > 1$, or a bifurcated solution. However, we have shown that the former is not an entropy maximum, so that the equilibrium state must be then a bifurcated solution. It was argued that the bifurcated solutions with $k > 1$ are probably not entropy maxima, then the parameter C would be uniquely determined by (14) with $k = 1$.

Consider the example of a very thin initial vorticity strip, nearly a vortex sheet. Suppose the velocity is equal to 1 on one side and -1 on the other side of this sheet, so that the circulation is 4π. The kinetic energy is then equal to $\frac{1}{2}$ multiplied by the domain area $4\pi L$, so that $\mathscr{E} = L/8\pi$. Therefore we predict a bifurcated final state with $\log C = \frac{1}{2}$. A wider strip would have lower energy, but then it would not lead to the dilute case, and our explicit solutions would not apply. A lower energy can be obtained with two vortex sheets at y positions $y = +d$ and $-d$. Then the velocity is equal to -1 for $y < -d$, 0 for $-d < y < +d$, and $+1$ for $y > +d$. With the same circulation as a single vortex sheet, the energy will be now equal to $2\pi\,(L-d)$, so that $\mathscr{E} = (L-d)/8\pi$. Therefore, if $d < 1$, bifurcated solutions with $\log C < \frac{1}{2}$ are obtained, and if $d \geqslant 1$, an x-independent final flow is predicted. Solutions with $\log C \geqslant \frac{1}{2}$ can be reached if the initial condition is of isolated vortices which contain more energy than vortex sheets.

The different solutions can thus be obtained from realistic initial conditions. These results can be understood by the following heuristical argument. The initial vorticity tends to diffuse as much as possible into the surrounding irrotational fluid. However, such a mixing would tend to decrease the energy, and a final equilibrium state is reached after a limited diffusion. If the initial energy is high, the system 'prefers' to diffuse at some places, and makes up for the corresponding loss of energy by forming vortices with high energy.

3. Vorticity mixing in a shear layer: a numerical test of the theory

3.1. *Numerical model*

The fluid motion is described by the Navier–Stokes equations written in terms of velocity and pressure

$$\left.\begin{aligned} &\frac{\partial \boldsymbol{u}}{\partial t} + (\boldsymbol{u}\cdot\boldsymbol{\nabla})\,\boldsymbol{u} = -\boldsymbol{\nabla} p + \nu\,\boldsymbol{\nabla}^2\boldsymbol{u}, \\ &\boldsymbol{\nabla}\cdot\boldsymbol{u} = 0 \end{aligned}\right\} \tag{16}$$

in the square domain $\Omega =]0, 2\pi[\times]-\pi, \pi[$. We use periodic boundary conditions in the x-direction and free-slip conditions ($\partial u/\partial y = 0$, $v = 0$) on the velocity at the boundaries $y = \pm\pi$. The initial condition consists of a basic x-wise velocity field upon which a perturbation is added (see §3.3). The basic velocity field is equal to $+1$ at $y = +\pi$ and -1 at $y = \pi$. We define the Reynolds number as $1/\nu$.

In order to ensure energy conservation, (16) was rewritten using the vector identity ($\boldsymbol{u}\cdot\boldsymbol{\nabla}\,\boldsymbol{u} = \boldsymbol{\omega}\times\boldsymbol{u} + \boldsymbol{\nabla}\,(\frac{1}{2}|\boldsymbol{u}|^2)$). The spatial derivatives and nonlinear terms of the equations are then treated numerically using a pseudo-spectral method (see Gottlieb & Orszag 1977). The spatial derivatives are computed in Fourier space while the nonlinear terms are evaluated in physical space. The components of the velocity are expanded in truncated exponential Fourier series in x, thus satisfying the periodicity conditions. The free-slip boundary conditions are attained by expanding u in a truncated sine series in y and v in a truncated cosine series, therefore achieving a y-periodic condition with symmetry (in the double domain). The cutoff wavenumber

$k_{\max}$ is equal to $\pi/\mathrm{d}s$, where $\mathrm{d}s$ is the grid size. (For the 256×257 resolution, with which all numerical simulations were carried out, $k_{\max} = 128$). The aliasing errors due to the computation of the nonlinear terms in physical space are removed by the method outlined in Patterson & Orzag (1971).

The divergence-free condition is imposed while solving the equation for the pressure field in Fourier space. We checked that the divergence of the velocity field always remains smaller than 10^{-10} in all of our numerical simulations.

The time advancement scheme is a third-order Adams–Bashforth scheme. Finally, the viscous terms are computed explicitly, because the stability condition is imposed by the advective timescale (and not by the diffusive timescale) as soon as the Reynolds number is large enough.

Choice of the numerical parameters

(i) Spatial resolution: the highest spatial resolution is of course desirable in order to reach high Reynolds number and properly handle the initial vorticity discontinuity. We chose 256^2 which allows to approach the inertial limit with reasonable computing time, in spite of the big number of iterations.

(ii) Time step: We have chosen $\mathrm{d}t = 0.005$ for all the runs.

(iii) Reynolds number: Since the typical velocity and width of the observed vortices are unity, $Re = 1/\nu$ is the actual Reynolds number as mentioned above. We try the highest Reynolds compatible with our resolution. When this parameter is too high, the calculation is less accurate at small scales, as demonstrated by a set of tests described in §3.2.

3.2. *Rate of decay of the integral quantities*

We shall now consider the effect of viscosity on the constants of the motion of the Euler equation. Simple manipulations lead to the classical balance equation for the energy

$$\frac{\mathrm{d}E_c}{\mathrm{d}t} = -\nu \Gamma_2. \tag{17}$$

Since Γ_2 (twice the enstrophy) always decays (see below), it is bounded by its initial value, so that the rate of energy dissipation vanishes in the limit of small viscosity ν. The difference between the energy at the end of the computation and its initial value is then a good indication of the influence of viscosity on the dynamics.

The evolution equation for the total circulation is obtained by direct integration of the Laplacian term

$$\frac{\mathrm{d}\Gamma_1}{\mathrm{d}t} = \nu \int_0^{2\pi} [\partial_y \omega]_{-L}^{+L} \mathrm{d}x.$$

Since the vorticity vanishes at the walls $y = \pm L$, and is negative inside the domain, $\partial_y \omega$ must be negative at $y = -L$ and positive at $y = +L$. Therefore Γ_1 can only decay in absolute value. However, the vorticity region generally does not reach the walls in our calculations, so that the circulation is virtually conserved.

The equation for the other momenta Γ_n is obtained by part integration of the viscous term $\nu n \omega^{n-1} \nabla^2 \omega$

$$\frac{\mathrm{d}\Gamma_n}{\mathrm{d}t} = -n(n-1)\nu \int_\Omega (\nabla \omega)^2 \omega^{n-2} \mathrm{d}x. \tag{18}$$

Since the vorticity is everywhere of the same (negative) sign, it is clear from this relation that all the moments must decay in absolute value. Direct verification of

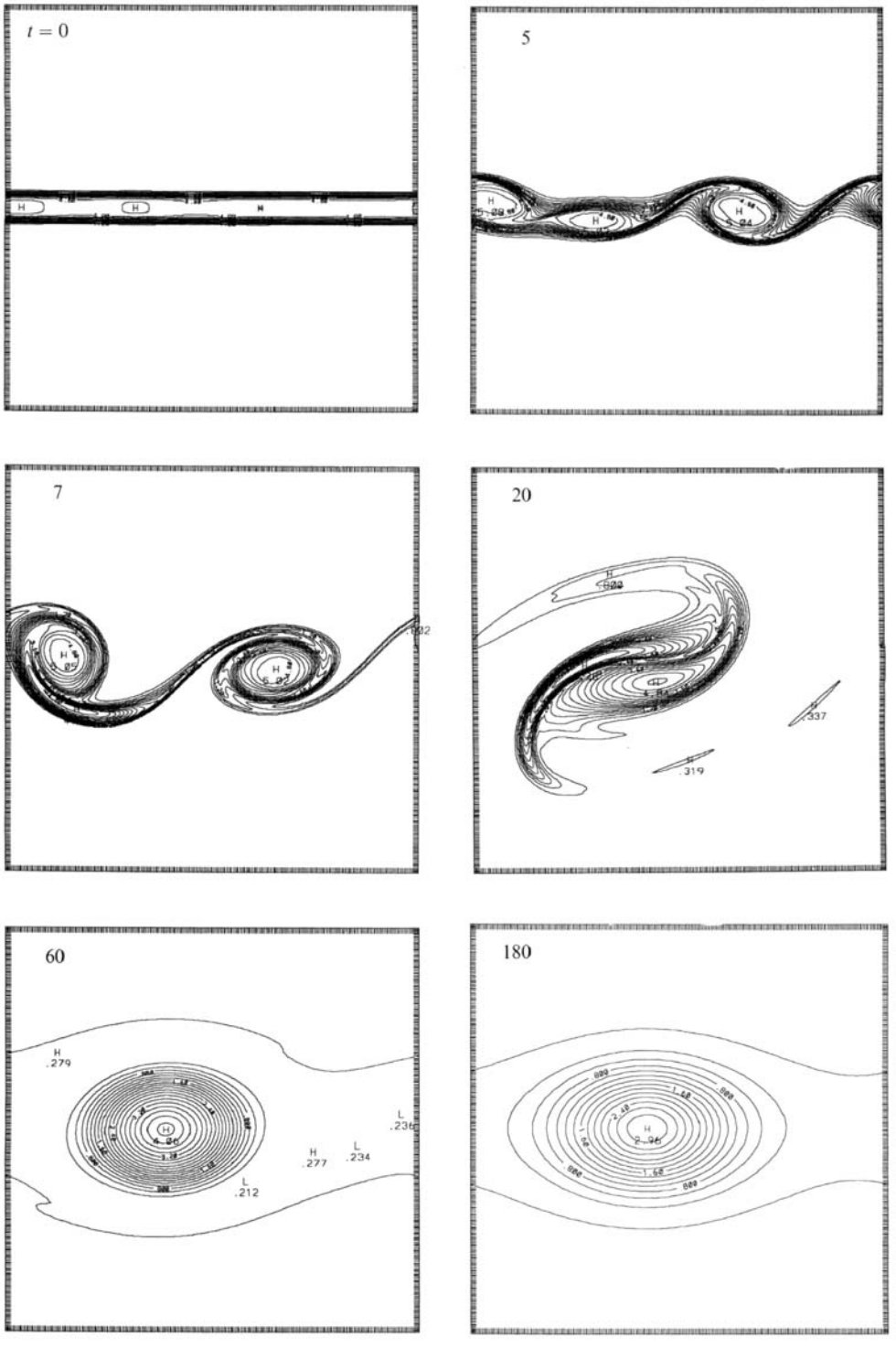

FIGURE 2. Successive snapshots of the vorticity field ($\delta = 0.215$, $Re = 1500$). The contour interval is 0.3 for $t = 0$ to 20, and 0.2 for $t = 60$ and 180.

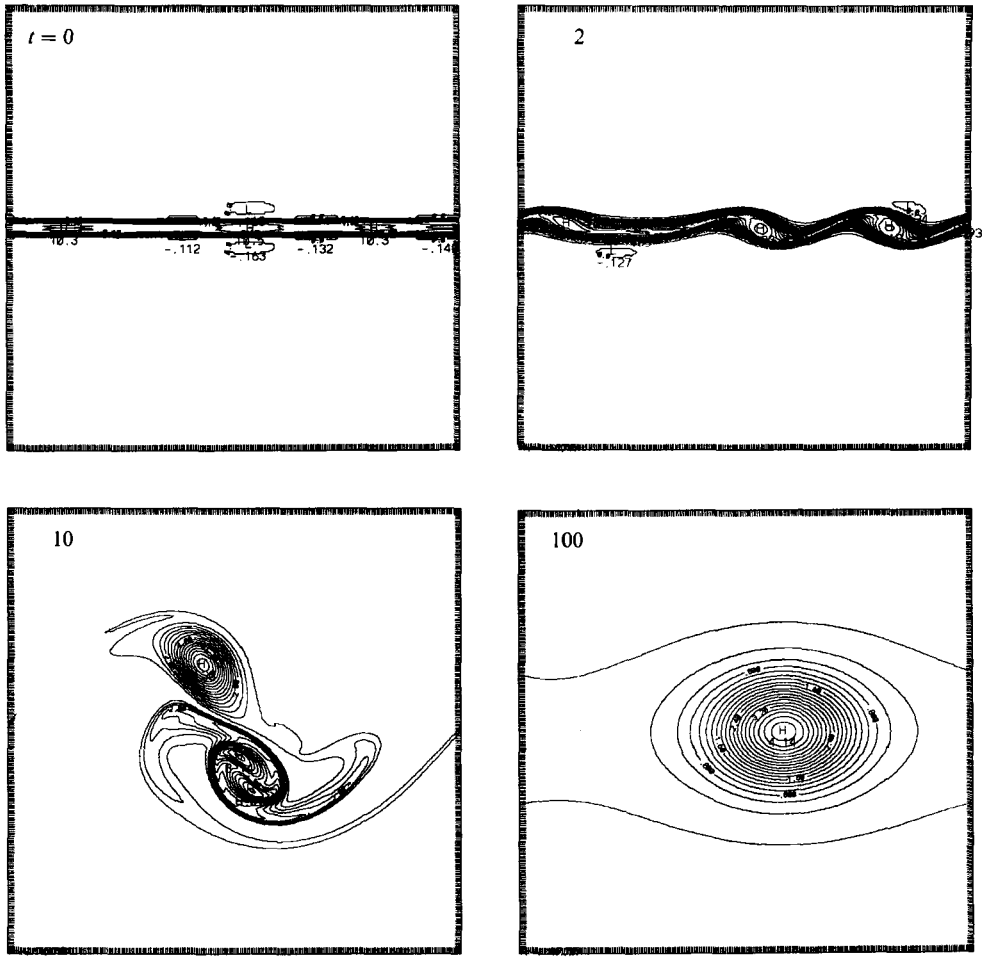

FIGURE 3. Successive snapshots of the vorticity field ($\delta = 0.1075$, $Re = 1200$). The contour interval is 0.6 for $t = 0$ and 2, 0.5 for $t = 10$, and 0.2 for $t = 100$.

these relations for the dissipation rates provides an indication that the computation accurately represents the mixing process. Therefore we calculate for each run the relative errors

$$\Delta_E = 1 + \frac{\mathrm{d}E_c}{\mathrm{d}t}\frac{1}{\nu\Gamma_2}, \quad \Delta_{\Gamma_n} = 1 - \frac{\mathrm{d}\Gamma_n}{\mathrm{d}t}\frac{1}{D_n},$$

where D_n is the theoretical expression for the dissipation rate. The time derivatives are calculated from the numerical fields by a second-order scheme.

The maximum of the vorticity field must always decrease, since it corresponds to a negative value of the Laplacian of ω. Similarly the minimum must increase. These properties provide very convenient tests of the calculation.

3.3. *Evolution of a single shear layer*

A typical flow evolution of the shear layer is represented in figure 2 by snapshots of the vorticity field. A chain of vortices first forms by shear instability, then a sequence of vortex merging occurs, and the flow slowly stabilizes into a final vortex structure, which very slowly diffuses by viscosity. We study the influence of the half-width δ

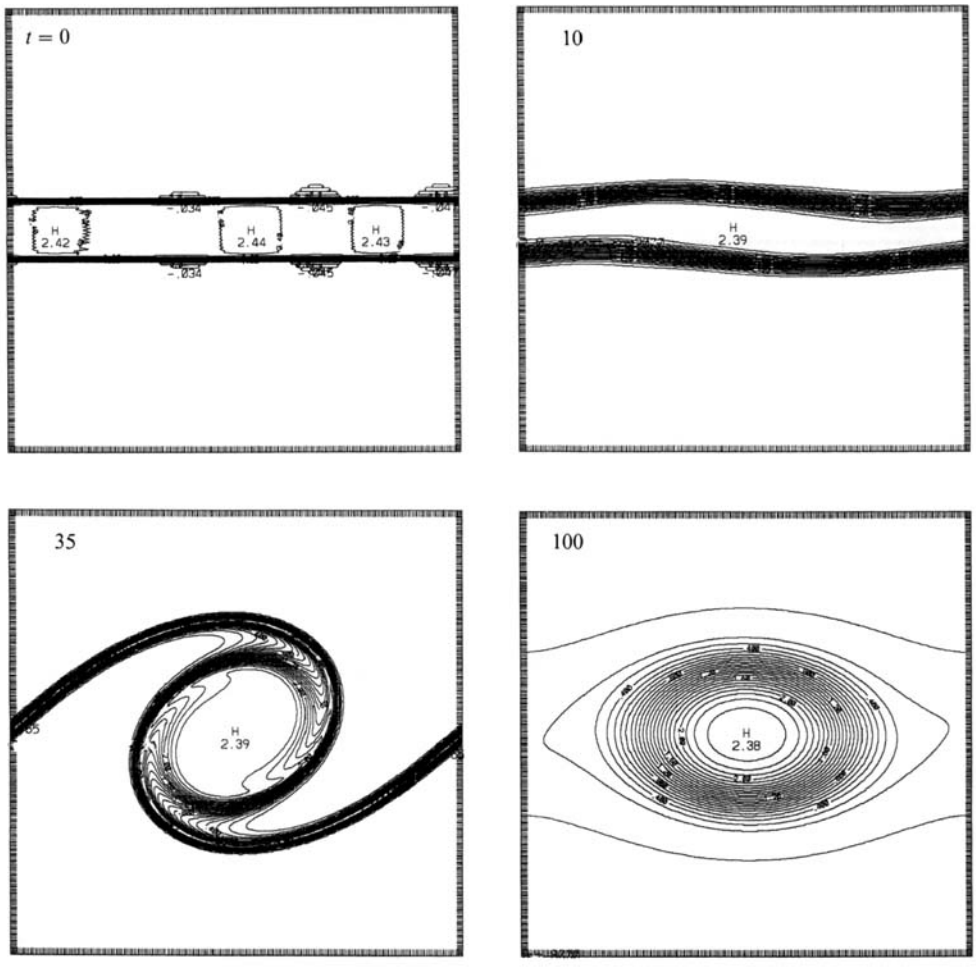

FIGURE 4. Successive snapshots of the vorticity field ($\delta = 0.43$, $Re = 1500$). The contour interval is 0.1.

of the vorticity strip, and the Reynolds number Re, as summarized in table 1 below. We now consider in detail the initial condition and the successive phases of the evolution.

3.3.1. *Initial condition*

We are interested in the evolution of a strip of uniform vorticity surrounded by irrotational fluid. The strip is oriented along the x-direction and centred at $y = 0$. This is the classical configuration of a shear layer: the velocity is directed along the x-axis and uniform outside the vorticity strip, with a negative velocity in the lower part and a positive one in the upper part. Since the numerical code cannot deal with a discontinuous vorticity field, we approach such a uniform strip by a continuous vorticity field, defined as

$$\omega(y) = -\frac{1}{\delta\Gamma(1+1/2m)}\exp\left(-(y/\delta)^{2m}\right).$$

This function tends to a vorticity strip in the limit of large m, and has a Fourier spectrum with exponential decay at high wavenumbers, which is appropriate for

δ	0.1075	0.215	0.215	0.215
Re	1200	750	1200	1500
m	3	3	3	3
ϵ	0.005	0.005	0.005	0.005
$E(0)$	0.489	0.478	0.478	0.478
$\delta_{100}E/E(0)$ (%)	13	15.7	11.3	9.4
$\delta_{100}E \times Re$		56.2	64.7	68.2
$\max(\lvert\Delta_{\Gamma_2}\rvert)$ (%)	3.7	2.0	2.1	2.5
$\max(\lvert\Delta_{\Gamma_{10}}\rvert)$ (%)	24	8.6	9.2	12
$\mu \times 10^4 (t = 100)$	0.82	2.08	0.87	0.37
$C(t = 100)$	2.64	2.31	3.33	5.0
δ	0.215	0.3225	0.43	2×0.215
Re	2000	1200	2000	1500
m	3	4	10	3
ϵ	0.005	0.005	0.0025	0.0025
$E(0)$	0.478	0.467	0.455	0.409
$\delta_{100}E/E(0)$ (%)	7.7	8.1	5.7	5.9
$\delta_{100}E \times Re$	71.8			
$\max(\lvert\Delta_{\Gamma_2}\rvert)$ (%)	2.1	1.2	1.3	1.3
$\max(\lvert\Delta_{\Gamma_{10}}\rvert)$ (%)	6.5	2.7	2.5	2.7
$\mu \times 10^4 (t = 100)$	0.25	0.87	0.05	5.10
$C(t = 100)$	5.99	4.0	16	2.0

TABLE 1. The parameters of the main runs

numerical differentiation. The main parameter that we vary is the half-width δ. The normalization factor, involving the gamma function Γ, is such that the integral of $\omega(y)$ is -2, in order to maintain for all cases the condition that $u = +1$ at large positive y and $u = -1$ at large negative y. The vorticity a at $y = 0$ is the inverse of this normalization factor (a is negative) and is uniform in most of the strip $-\delta < y < +\delta$.

Such a flow is a steady solution of the Euler equations, but it is generally unstable. Adding explicitly a small perturbation allows the instability to be controlled and initiated more quickly, before a significant viscous diffusion of the vorticity profile can occur. We chose a perturbation with components in the Fourier modes 1, 2, 3 and 4 with arbitrary phases. The perturbation is confined to the neighbourhood of the vorticity strip by an exponential factor in the y-coordinate. We have checked that, while the sequence of merging processes and the position of the final vortex depend on the phases and relative amplitude of the four modes, the structure of the final state does not vary significantly. We have then chosen to keep the same perturbation shape for comparing the different cases presented in this section, and it is obtained from the stream function:

$$\psi_p = \epsilon \exp\left(-\frac{y^2}{4\delta^2}\right)[0.5\sin(x-\tfrac{1}{2}\pi) + 0.5\sin(2x) + \sin(3x-\phi_3) + 0.5\sin(4x)]. \quad (19)$$

We use $\epsilon = 0.005$ or $\epsilon = 0.0025$ and $\phi_3 = \frac{1}{2}\pi$.

3.3.2. *The initial instability*

The first phase of the evolution is the formation of a chain of vortices as the result of the shear instability. The number of vortices that develop can be estimated by an inviscid linear stability analysis, using Rayleigh's equation. For a strip with uniform vorticity, the growth rate of a wavenumber k starts from zero at $k = 0$, reaches a

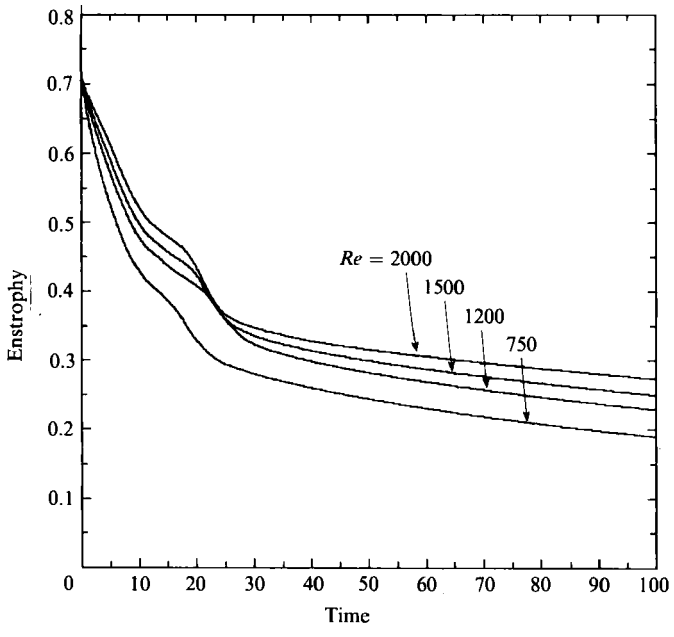

FIGURE 5. The enstrophy decay for different Reynolds numbers with the same initial condition ($\delta = 0.215$).

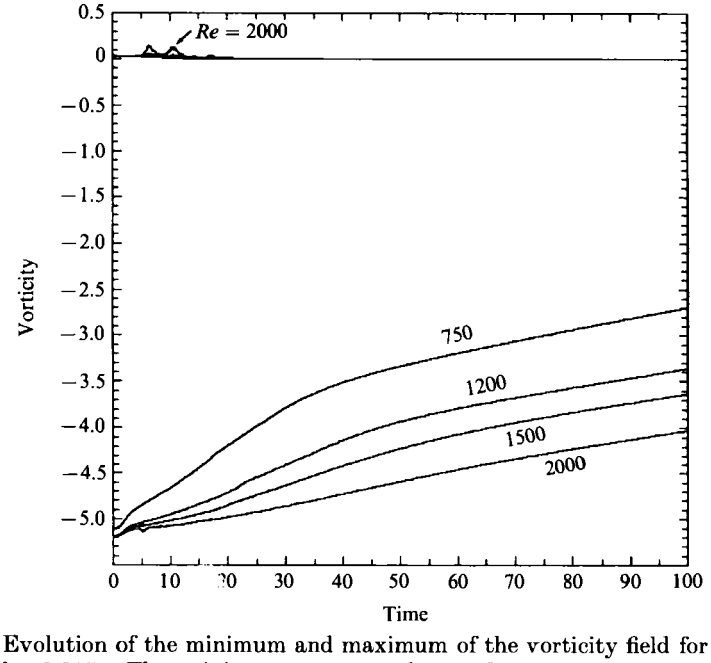

FIGURE 6. Evolution of the minimum and maximum of the vorticity field for different Reynolds numbers ($\delta = 0.215$). The minimum corresponds to the vortex centre, and the maximum corresponds to the irrotational surrounding fluid. All the curves for the maxima are close to 0 except at $Re = 2000$, for which spurious fluctuations appear.

maximum at $k\delta \approx 0.40$, and vanishes at $k\delta \approx 0.64$, so that the perturbations with higher wavenumbers do not grow (see e.g. Drazin & Reid 1981). In the case of a Gaussian vorticity profile ($m+1$), the behaviour is qualitatively the same but these two numbers become respectively 0.495 and 1.04 (from Hazel 1972). For intermediate

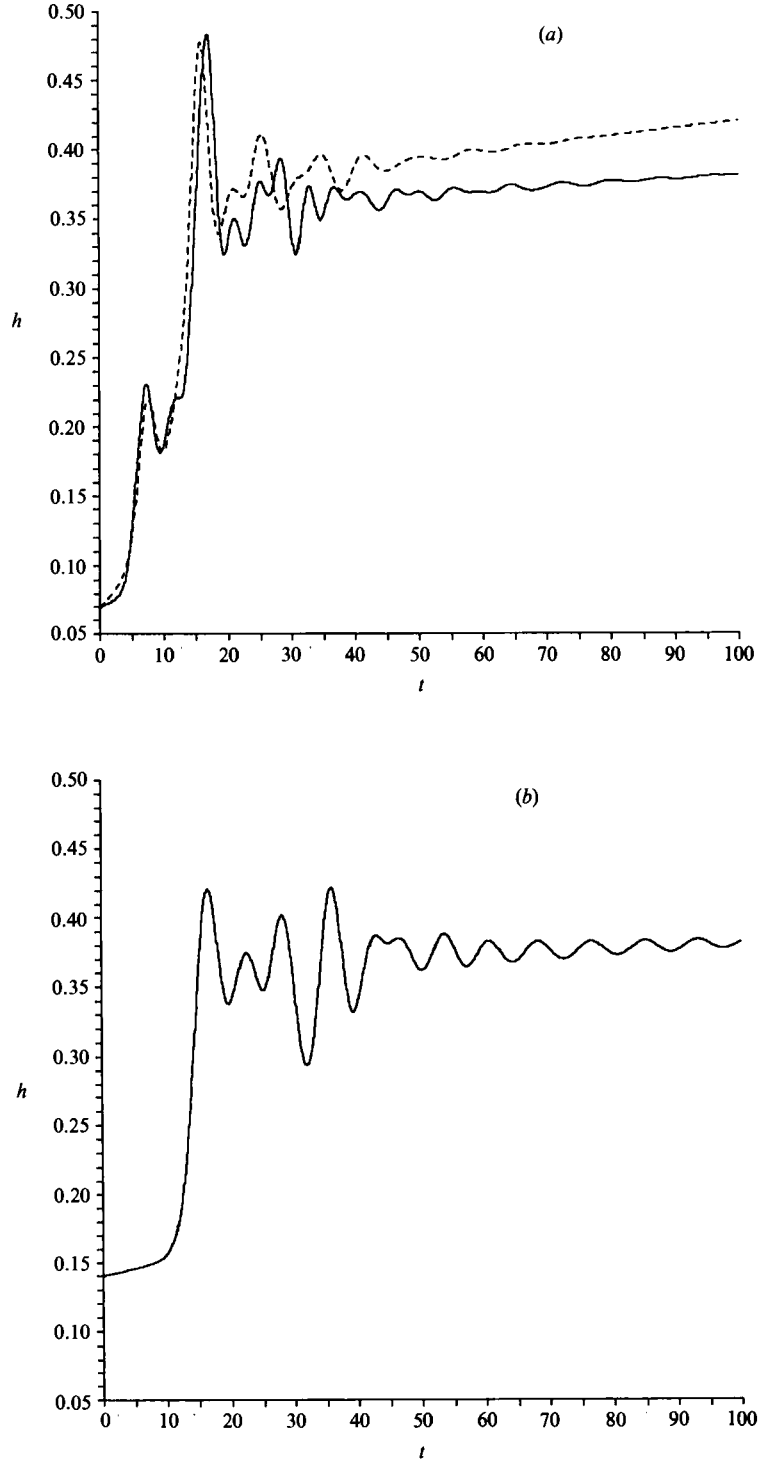

FIGURE 7. Evolution of the momentum thickness h: (*a*) $\delta = 0.2150$, for $Re = 750$ (dashed) and $Re = 2000$ (solid). The global decay of the oscillations does not depend significantly on viscous effects. (*b*) $\delta = 0.43$, $Re = 2000$.

values of m, the results should be between these two cases. The periodic boundary conditions restrict the wavenumbers to integer values. Thus, for $\delta = 0.215$, the wavenumber $k = 3$ is about marginal, and $k = 2$ is the most amplified. We indeed observe (figure 2) a chain of three vortices, but two vortices quickly dominate. For $\delta = 0.1075$ the four vortices initially grow as expected (figure 3), while for $\delta = 0.43$, only the mode $k = 1$ can grow (figure 4). For $\delta > 0.64$ (and m large), the flow must be stable, since the first allowed mode $k = 1$ is already beyond the range of instability. We have indeed checked that for $\delta = 0.645$, the vortex strip is stable, and grows only by a slow viscous diffusion.

3.3.3. *Merging and relaxation toward the final vortex*

When several vortices form, they quickly undergo merging processes. Because of the initial perturbations, this merging occurs quickly and does not only involve pair interactions, but also more complex interactions. After this merging a single vortex slowly relaxes towards an equilibrium state. (The flow should rather be thought as a chain of vortices, in which any further merging is forbidden by the periodic boundary condition in x.) The vortex then slowly diffuses, but on a much longer timescale. Since the vortex scale is about unity, this diffusive timescale is of the order of the Reynolds number, which is at least an order of magnitude longer than the time for inertial organization. Our purpose is to analyse this inertial equilibrium state and compare it with the prediction of the statistical theory. However it is also important to investigate the transient evolution to test the numerical computation and monitor the mixing process.

We first observe that the total energy of the flow always slowly decays, as it should. The initial energy (divided by the domain area $4\pi^2$) is indicated for the different runs in table 1 at time $t = 0$. This initial energy is a little less than $\frac{1}{2}$, the limit for a vorticity sheet. The energy loss at $t = 100$, defined as $\delta_{100} E = E(0) - E(100)$, indicates the influence of viscous effects. The ratio of this energy loss to the total initial energy is indicated in the table, and is typically 10%, which is reasonably small. The influence of the Reynolds number has been carefully investigated in the case $\delta = 0.2150$. We notice that the product of the energy loss and the Reynolds number apparently tends to a constant as Re is increased. This means, from (17), that the enstrophy must become independent of the Reynolds number. We check in figure 5 that the enstrophy evolution is indeed very close for $Re = 1500$ and $Re = 2000$, confirming that we are reaching the inertial limit.

As a test of the computation, we have directly checked (17) and (18) for the dissipation rates of the integral quantities, by plotting the evolution of the errors Δ_E, Δ_{Γ_2} and $\Delta_{\Gamma_{10}}$ defined in §3.2. The relative error Δ_E is always smaller than 10^{-3}. The errors Δ_{Γ_2} and $\Delta_{\Gamma_{10}}$ oscillate around 0 and their maximum excursion is indicated in the table. The precision on the enstrophy dissipation term is a few percents. The precision on the higher vorticity moment is somewhat less good especially for a narrow initial vorticity strip. Surprisingly, these errors do not increase with Re, so they cannot be used as a test for the choice of the optimum Reynolds number.

As mentioned in §3.2, the maximum of the vorticity field must decay while the minimum must grow in the mixing process. These two quantities are plotted on figure 6 for different Re ($\delta = 0.2150$). The minimum is not exactly zero because of the small initial perturbation. For $Re = 2000$, these quantities fluctuate slightly in the initial phase of the evolution. This spurious behaviour reveals that the Re is slightly too high for a precise computation of the viscous term. (However, the evolution of the global quantities, as represented on figures 5 and 7, is still probably fairly

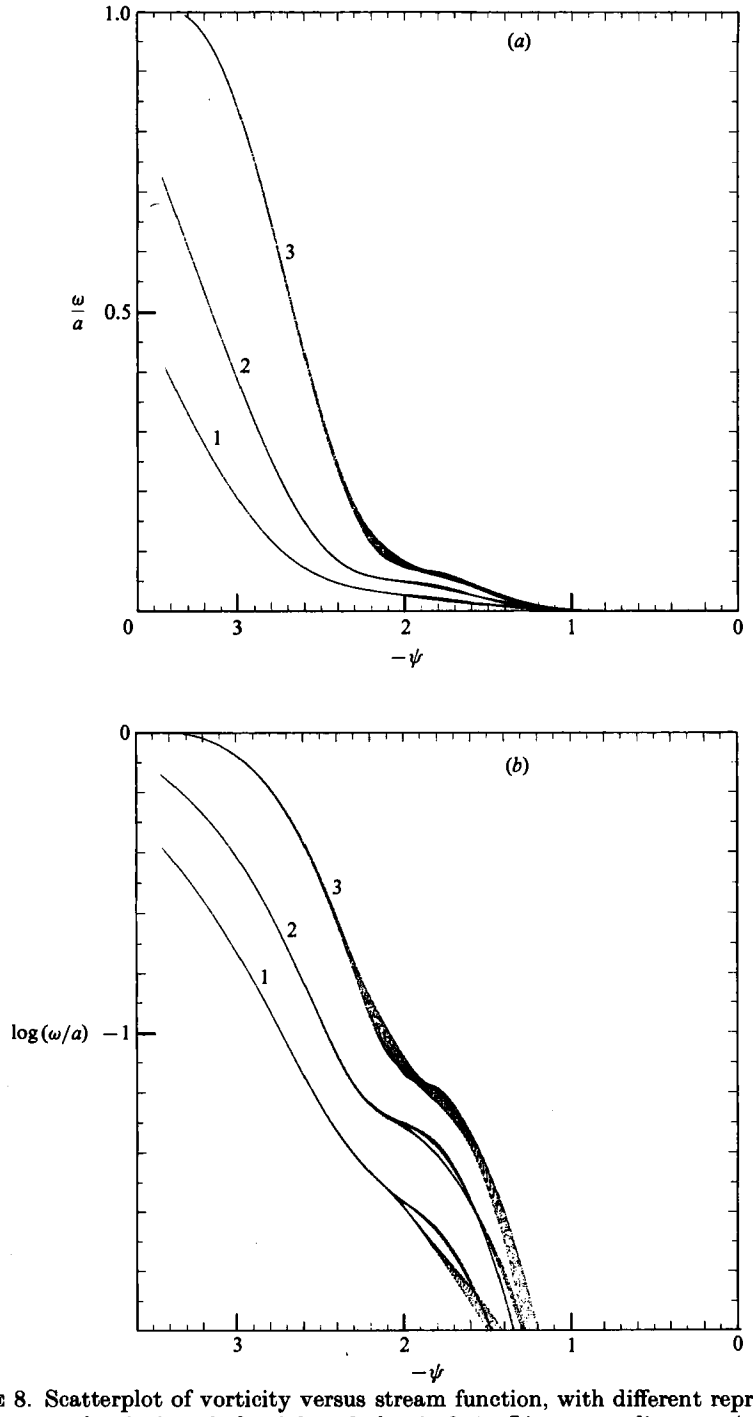

FIGURE 8. Scatterplot of vorticity versus stream function, with different representations (at $t = 100$): curve 1, $\delta = 0.1075$; 2, $\delta = 0.215$; 3, $\delta = 0.43$. (*a*) Linear coordinates ω/a and ψ, (*b*) log ω/a versus ψ.

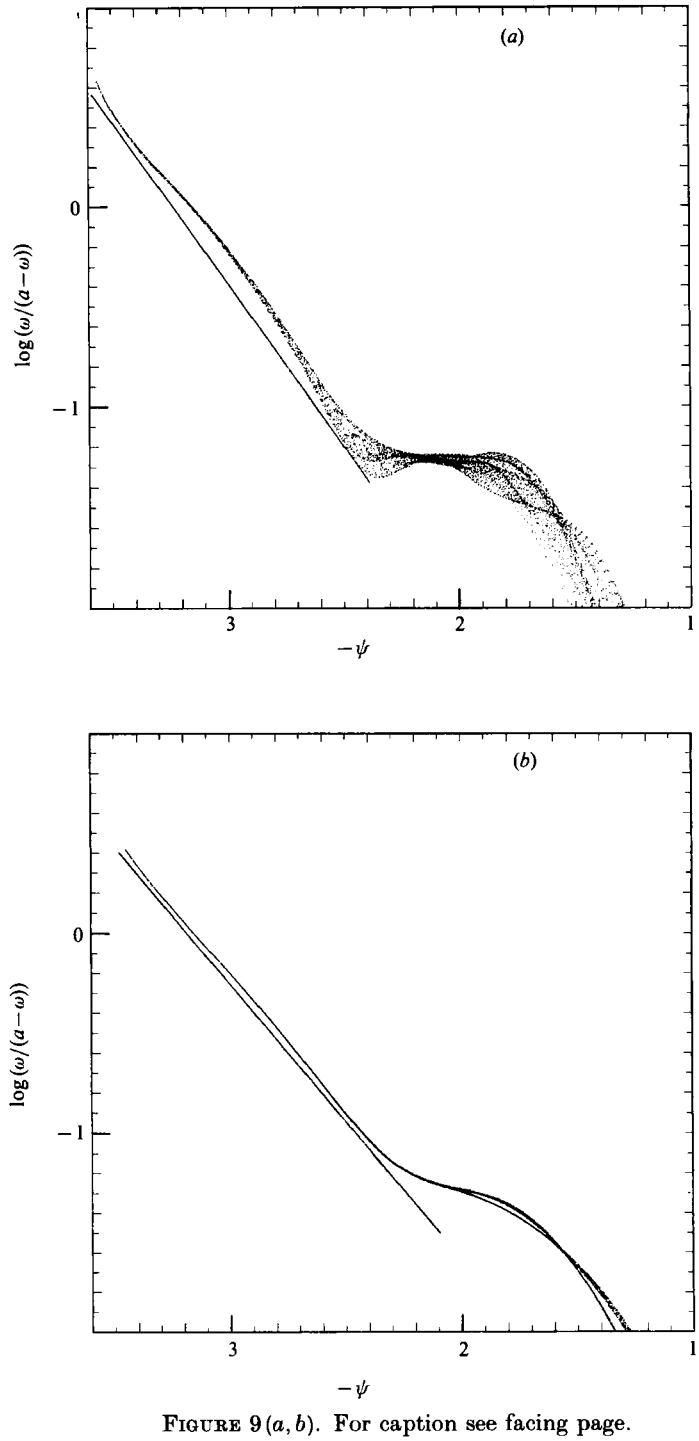

FIGURE 9(a, b). For caption see facing page.

accurate at $Re = 2000$.) By contrast, the fluctuations are virtually absent for Re below 1500. This appears to be a very accurate test of the computation, probably because it probes locally the regions with high excitation. We can conclude that computations with $Re < 1500$ are quite reliable for a precise study of vorticity

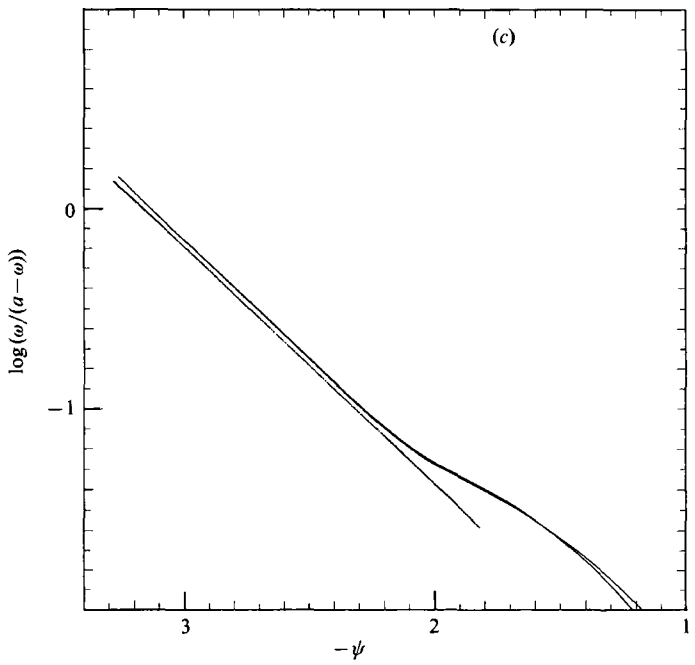

FIGURE 9. Scatterplot of log $(\omega/a-\omega))$ versus stream function ψ at different times in the equilibrium regime for $\delta = 0.215$: (*a*) $t = 60$, the fitted parameters are $\mu = 1.2\times10^{-5}$ and $C = 5.96$; (*b*) $t = 100$, fitting $\mu = 3.7\times10^{-5}$ and $C = 5.0$; (*c*) $t = 180$, fitting $\mu = 19.9\times10^{-5}$ and $C = 2.35$. (To reduce the size of the figures, we have removed the points with a stream function between 0 and -1, where the vorticity is virtually zero.)

structures. This test is used to find the optimal Reynolds number for the other initial conditions.

The mixing process is classically characterized by the evolution of the momentum thickness, defined in our case by

$$h = \tfrac{1}{4}\int_{-L}^{+L} (1-\langle u\rangle)(1+\langle u\rangle)\,\mathrm{d}y,$$

which indicates the width of the region where the x-averaged velocity $\langle u\rangle(y)$ significantly departs from the values 1 or -1 in the far distance. Notice that the kinetic energy of the x-averaged velocity is equal to $\frac{1}{2}-2h$. The momentum thickness (figure 7) increases owing to the growth of the shear instability and merging, then undergoes a series of damped oscillations until the steady regime with slow viscous diffusion is reached. The damping time of the oscillations depends on the initial condition as shown on the two examples of figure 7. It is important to notice that the damping and the relaxation to an equilibrium state are controlled by inertial effects, not by viscosity: indeed the rate of damping seems very similar at $Re = 750$ and $Re = 2000$ (for $\delta = 0.2150$). However, a precise characterization of this damping is not easy since several periods of oscillation coexist.

3.4. *The final state of a single shear layer*

We study the final state by representing each point of the computation grid on a scatterplot with abscissa ψ and ordinate ω. For a steady solution of the Euler equation, all these points must collapse on a curve, or a set of curves. In our case, we

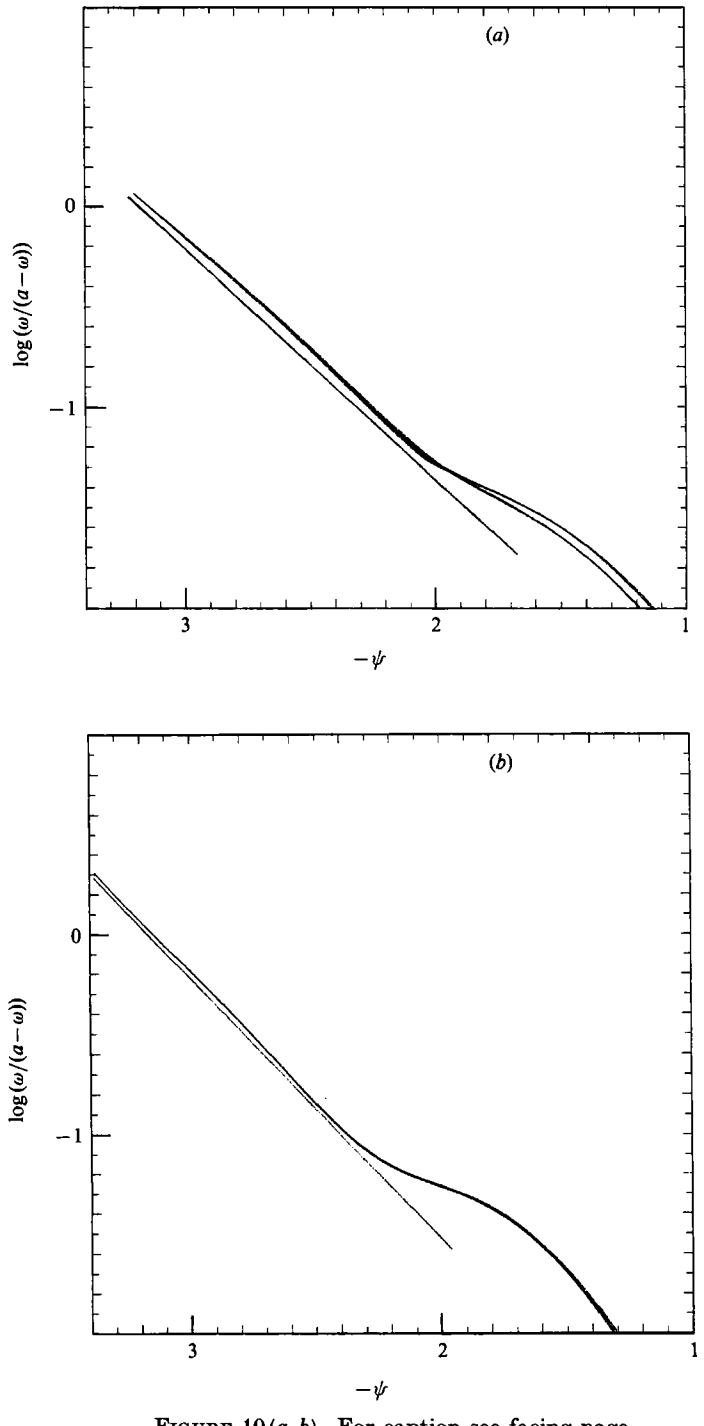

FIGURE 10(a, b). For caption see facing page.

obtain a family of closed streamlines in the vortex, and a family of 'open' streamlines outside it (in fact they are closed by the periodic boundary condition). On each side of the shear layer there are two open streamlines for a given value of the stream function; therefore the relation $\omega = f(\psi)$ can have two branches in this region.

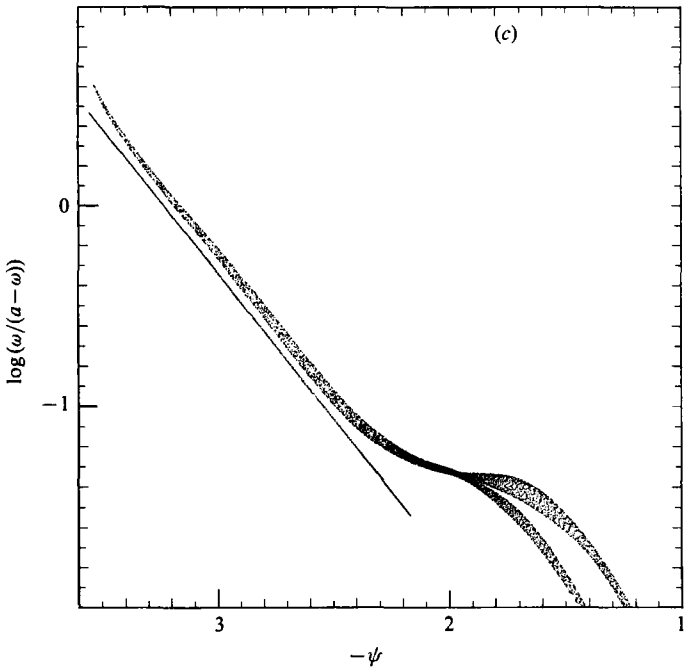

FIGURE 10. Equilibrium structures at $t = 100$ for different Reynolds numbers ($\delta = 0.215$): $\log(\omega/a-\omega))$ versus ψ. (*a*) $Re = 750$, (*b*) $Re = 1200$, (*c*) $Re = 2000$.

Scatterplots at time $t = 100$ are given in figure 8 for different initial conditions. Since the points nearly collapse onto curves, the system is indeed very close to a steady Euler flow. The upperpart of the curve corresponds to the closed streamlines inside the vortex, while the low part represents the open streamlines in the outer region with low vorticity. The curves behave as predicted by (7): an hyperbolic tangent with asymptotes at $\omega = 0$ and a. Of course the curve is limited to the interval of variation of ω, so that the saturation at $\omega = a$ appears only for an initial condition with a wide strip. For a narrow initial strip we keep only the lower part of the tanh function, which is close to an exponential (curve 1 of figure 8*b*), as expected in the dilute case, or with Onsager's theory.

A quantitative test of the theory is performed by plotting $\log(\omega/(a-\omega))$ versus ψ, which must be a straight line according to (7). The agreement is indeed excellent inside the vortex, as shown in figure 9($\delta = 0.215$, $Re = 1500$). The curve first oscillates around a straight line, and then clearly tends to this linear relationship. Notice that a is taken as the extremum vorticity of the initial state ($a = -1/\delta\Gamma(1+\frac{1}{2}m)$), so there is no adjustable parameter in this representation. Outside the vortex we find a region of fairly uniform low vorticity, and still further the vorticity drops down very steeply. The mixing process has not reached this outer region.

We have checked that this behaviour is very similar at $Re = 1200$ (figure 10). At $Re = 750$, the agreement with theory becomes less good, which is not surprising since results on the enstrophy indicate that we are still far from the inertial limit. At $Re = 2000$ the agreement is still good except for a cusp at the vortex centre. However, the vortex did not quite reach a steady state, and the calculation is not as good in this case (the vorticity extrema fluctuate).

The agreement with theory is confirmed with a narrower initial strip (figure 11).

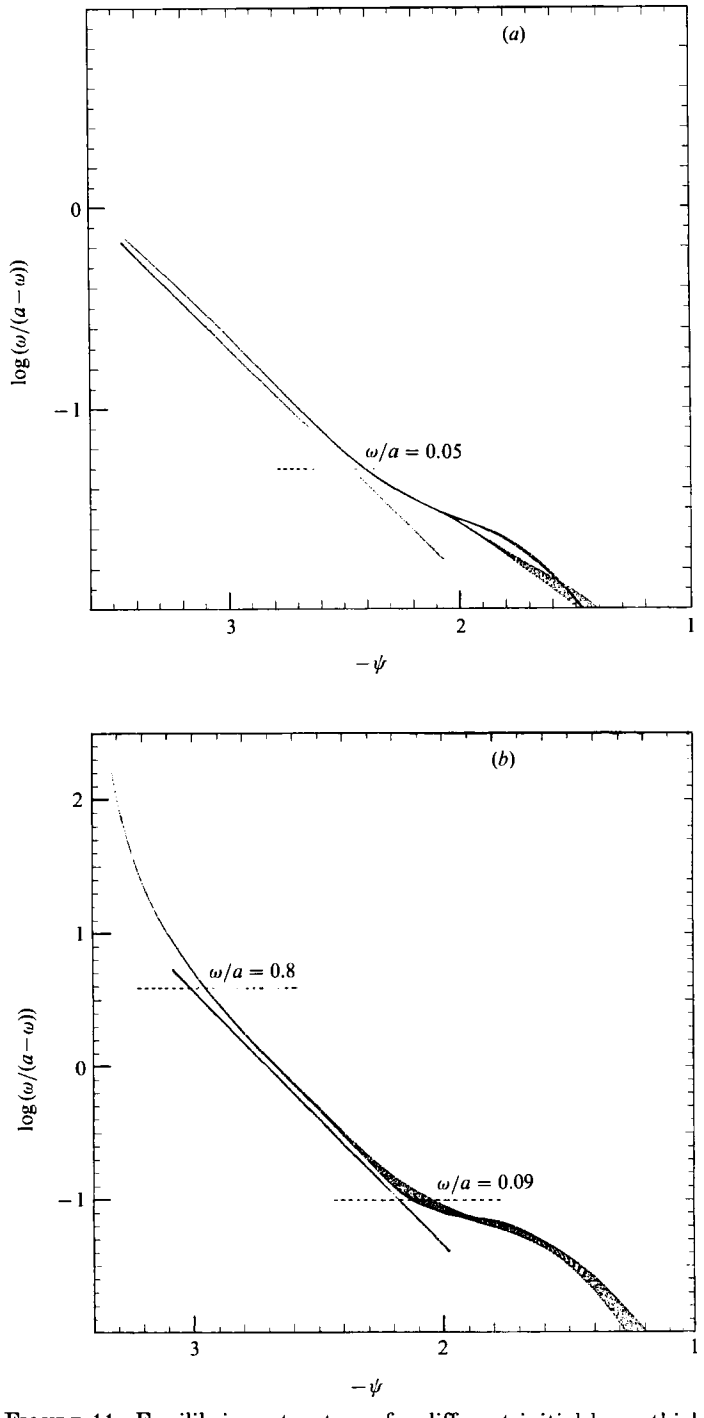

FIGURE 11. Equilibrium structures for different initial layer thicknesses: $\log(\omega/(a-\omega))$ versus ψ. (*a*) $\delta = 0.1075$, (*b*) $\delta + 0.43$.

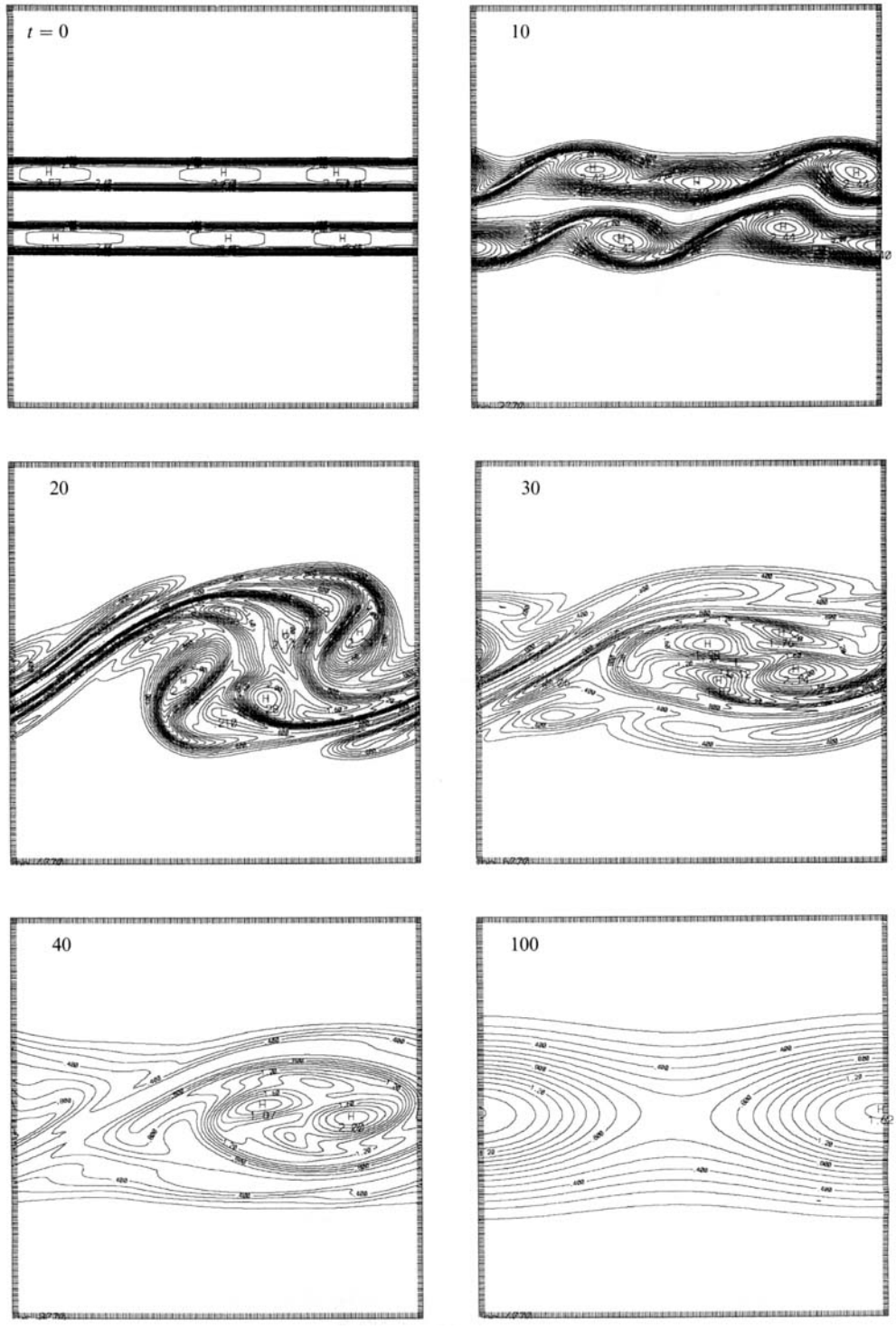

FIGURE 12. Successive snapshots of the vorticity field showing the evolution of a double shear layer.

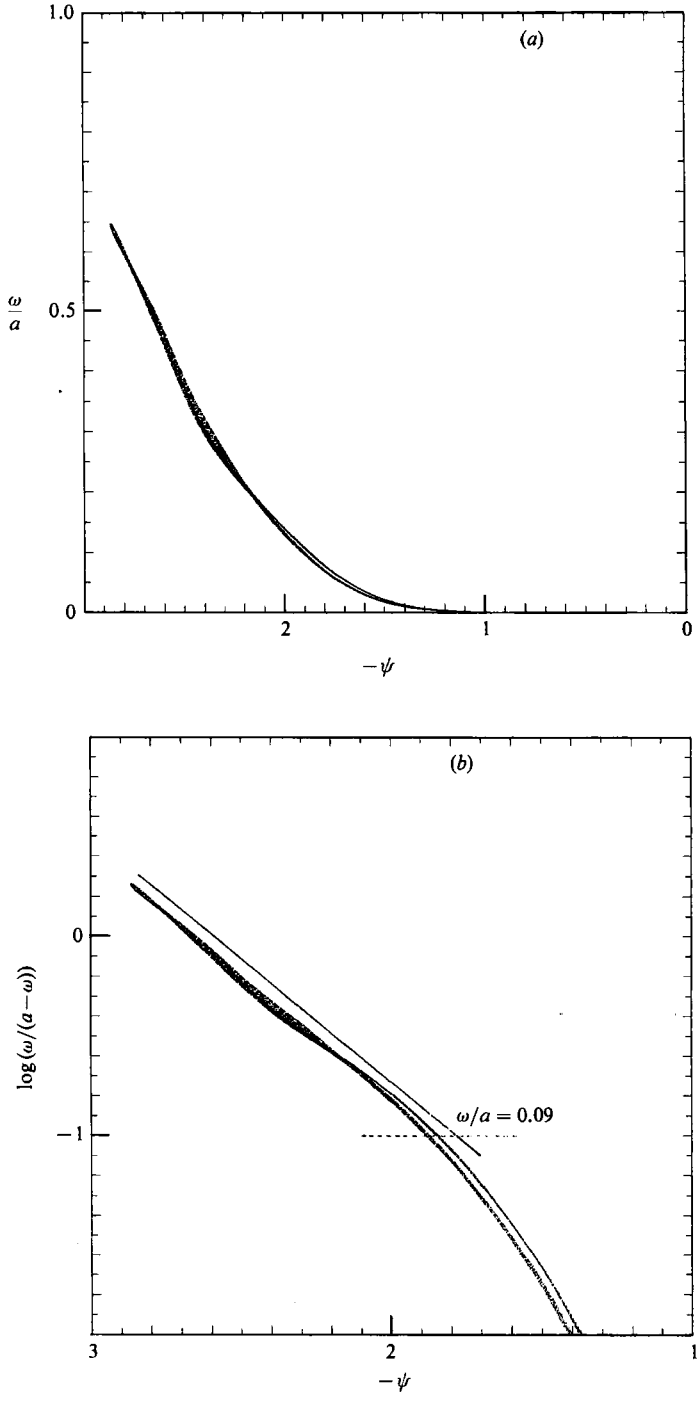

FIGURE 13. Equilibrium structure of the double shear layer at $t = 100$: (*a*) ω/a versus ψ, (*b*) $\log(\omega/a-\omega))$ versus ψ.

For a wide strip we still obtain a good agreement between $\omega/a = 0.1$ and $\omega/a = 0.8$, where strong vorticity mixing has occurred. However, we observe that the vorticity in the central region of the vortex remains too high: it does not mix sufficiently with the surrounding. Notice that the discrepancy with theory is exaggerated when we divide by the small quantity $\omega - a$: even in this central region of the vortex, the curve still behaves qualitatively like an hyperbolic tangent, as seen on curve 3 of figure 8(*a*).

The parameters λ and μ in (7) can be deduced from the straight line fitting. In table 1 we give μ and C, deduced from λ by (13) (with $k = 1$ and $L = \pi$). The parameter C has a clear meaning only in the dilute case, as it appears in (12). Then we obtain values much higher than the $e^{\frac{1}{2}} \approx 1.65$ predicted in §2.3. This discrepancy is not surprising since (7) is only satisfied in the vortex region, not in the whole domain. We observe that C slowly decreases with time as the vortex diffuses (figure 9), and it may tend to the theoretical value in the limit of very long time.

3.5. *The case of a double shear layer*

We have predicted in §2.3 that weaker vortices (corresponding to $\log C < \frac{1}{2}$), or even x-independent flows, should be obtained as the final state of a double initial shear layer. This initial condition corresponds to two thin vorticity strips centred at $y = -d$ and $+d$, with vorticity level $a = -\frac{1}{2}\delta$ and thickness 2δ for each, such that the lower and upper velocities are still -1 and $+1$. In practice, we add two smoothed strips with $\delta = 0.215$, and a perturbation (19) centred on each strip, with $\phi_1 = \frac{1}{2}\pi$ in the lower layer and $\frac{1}{3}\pi$ in the upper one, to avoid complete symmetry.

The evolution is illustrated in the case $d = \frac{1}{2}$ by the snapshots of figure 12. Each of the two shear layers first undergoes independent instability and merging. Then merging between the two layers occurs, leading to very complex mixing. We find that the final state is in agreement with theory (figure 13) in regions with vorticity higher than $0.09a$. As for a single shear layer, the mixing has not reached the whole domain. The parameter C (see table 1) is lower than in the runs with a single shear layer, as it should be, but it is still higher than the predicted value.

We have tried a similar calculation with $d = 1$, for which an x-independent final state was conjectured in §2.3. However, we have observed that each layer then develops fairly independently, and produces its final vortex. The interaction between these two vortices produces an x-wise steady translating motion of each vortex in opposite directions. Deformation of these vortices occurs when they pass each other, but it is not sufficient to produce merging, and the system does not converge to a steady state. Similar behaviour was obtained with a quadruple shear layer. Therefore it seems unlikely that an x-independent final state can be obtained, at least in a reasonable time. The system tends to achieve local equilibria into vortices faster than the global equilibrium. Notice also that we have only proved that the x-independent state is a critical point, not necessarily an entropy maximum beyond $qL = \frac{1}{8}\pi^{\frac{1}{2}}$. Since the expected x-independent state would correspond to a much larger value of q (close to 1), there may be no equilibrium state for the corresponding range of initial conditions.

4. Conclusions

In the case of an initial condition with two vorticity levels a and 0, the statistical theory predicts that, after complex mixing, the flow should tend to a steady state, characterized by the simple relationship (6) between vorticity and stream function.

We observe in the numerical computations that the flow tends to a steady state and the relationship between ω and ψ is in excellent agreement with theory in the regions where significant mixing between the two initial vorticity levels occur. Mixing occurs in a confined domain, so that the boundaries are important. However, in the cases that we consider here, the equilibrium vorticity distribution drops before reaching the walls $y = \pm L$, and the confinement is mostly due to the periodic boundary conditions in the x-direction. This would not be the case in a domain with a small aspect ratio.

We observe in the simulations that the mixing process does not cover the whole fluid domain. Far distant regions remain virtually irrotational, and if the initial vorticity strip is wide, a region of unmixed fluid, with nearly maximal vorticity, remains at the vortex centre. In these regions (6), fitted in the mixed part of the flow, is poorly satisfied. To allow a relevant comparison with theory, thin vorticity tongues must develop and be stirred in a complex way. Viscosity must smooth the vorticity only at the end of this process. With a moderate Reynolds number, this condition is achieved only in the regions of the flow with the most active stirring. It is therefore not surprising that the theory is less good in regions with nearly pure vorticity levels $\omega = 0$ or a. Formation of a local equilibrium in a fluid bubble is also observed at higher Re in laboratory realizations of isolated vortex structures, as in Nguyen Duc & Sommeria (1988).

The good agreement in the case of a double shear layer with $d = \frac{1}{2}$ confirms that the theory has a wide domain of validity. However, when the distance between the two strips is too large, we tend to get a vortex in each layer rather than the expected x-independent flow. Notice also that the x-independent flow was not proved to be a maximum entropy state in this case.

We must keep in mind that in our tests, we try to connect a statistical property of perfect fluids with the behaviour of simulated viscous fluids. Of course a complete agreement is conceivable only in the limit of high Re and very long times. Attempts to reach conditions of higher effective Reynolds numbers by replacing the Laplacian by a biharmonic viscosity did not lead to a good quantitative agreement with theory, although the general flow evolution is not strongly affected by this modification. Indeed the biharmonic term does not smooth out the local vorticity fluctuations: rather, it would smooth out the vorticity gradients. In particular the maximum and minimum of the vorticity field did not decay monotonically as they should. Therefore much care is required for quantitative tests of the theory.

A predictive use of the theory requires the resolution of (7), which must be done generally by numerical methods (but the spatial resolution does not need to be as high as in a direct numerical simulation at large Re). In the particular case of dilute vorticity, we meet Onsager's statistical theory of point vortices, with local averaging. Equation (7) is then solved explicitly, in the limit of a wide domain. We notice that the family of Stuart vortices is indeed a solution of the problem, which does not seem to have been noticed previously.

The theory relies on the local conservation of the vorticity ω and is therefore limited to two-dimensional flows. However, it is striking to notice that Stuart's vortices are often considered as a good representation of the organized structures which appear in ordinary turbulent shear layers (with three-dimensional eddies). This remark leads to a possible interpretation of these organized structures: they would be by far the most probable states in a strongly stirred flow: successive merging would correspond to successive stabilization in metastable states with higher and higher entropy. We

then conjecture that these organized structures could be states of statistical equilibrium rather than dissipative structures.

The computations have been performed on the CRAY2 of the CCVR (Centre de Calcul Vectoriel pour la Recherche) at Palaiseau. Computation time has been allocated by the Scientific Committee of the CCVR. An initial study of these organized structures was performed as one of us (J.S.) was visiting P. Rhines at Seattle, with the support of NSF Grant OCE-89-16009, and J.S. wishes to thank him for his encouragement.

REFERENCES

ANTIPOV, S. V., NEZLIN, M. V., SNEZHKIN, E. N. & TRUBNIKOV, A. S. 1986 Rossby autosolution and stationary model of the Great Red Spot. *Nature* **323**, 238–240.

CORCOS, G. M. & SHERMAN, F. S. 1984 The mixing layer: deterministic models of a turbulent flow. Part 1. Introduction and the two-dimensional flow. *J. Fluid Mech.* **139**, 29–65.

DRAZIN, P. G. & REID, W. H. 1981 *Hydrodynamic Stability*. Cambridge University Press.

GIDAS, B., NI, W. M. & NIRENBERG, L. 1979 *Commun. Math. Phys.* **68**, 203–243.

GOTTLIEB, D. & ORSZAG, S. A. 1977 *Numerical Analysis of Spectral Methods: Theory and Applications*. SIAM.

HAZEL, P. 1972 Numerical studies of the stability of inviscid stratified shear flows. *J. Fluid Mech.* **51**, 39–61.

LIOUVILLE, J. 1853 Sur l'équation aux différences partielles $\partial^2 \log\lambda/\partial u \partial v \pm \lambda/2a^2 = 0$. *J. Maths* **18**, 71–72.

MONTGOMERY, D. & JOYCE, G. 1974 Statistical mechanics of negative temperature states. *Phys. Fluids* **17**, 1139–1145.

NGUYEN DUC, J. M. & SOMMERIA, J. 1988 Experimental characterization of steady two-dimensional vortex couples. *J. Fluid Mech.* **192**, 175–192.

ONSAGER, L. 1949 Statistical hydrodynamics. *Nuovo Cimento suppl.* **6**, 279.

PATTERSON, G. S. & ORSZAG, S. A. 1971 Spectral calculations of isotropic turbulence: efficient removal of aliasing interactions. *Phys. Fluids* **14**, 2538–2541.

RABAUD, M. & COUDER, Y. 1983 A shear flow instability in a circular geometry. *J. Fluid Mech.* **136**, 291–319.

ROBERT, R. 1989 Concentration et entropie pour les mesures d'Young. *C. R. Acad. Sci. Paris*, I **309**, 757–760.

ROBERT, R. 1990 Etat d'équilibre statistique pour l'écoulement bidimensionnel d'un fluide parfait. *C. R. Acad. Sci. Paris* I **311**, 575–578.

ROBERT, R. 1991 Maximum entropy principle for two-dimensional Euler equations. *J. Statist. Phys.* (to appear).

ROBERT, R. & SOMMERIA, J. 1991 Statistical equilibrium states for two-dimensional flows. *J. Fluid Mech.* **229**, 291–310.

SOMMERIA, J., MEYERS, S. D. & SWINNEY, H. L. 1988 Laboratory simulation of Jupiter's Great Red Spot. *Nature* **331**, 689–693.

STUART, J. T. 1967 On finite amplitude oscillations in laminar mixing layers. *J. Fluid Mech.* **29**, 417–440.